Geophys. J. Int. (2001) **144,** 1–22

Stratified multifractal magnetization and surface geomagnetic fields—I. Spectral analysis and modelling

S. Lovejoy,[1] S. Pecknold[1] and D. Schertzer[2,3]

[1] *Department of Physics, McGill University,* 3600 *University St, Montréal, Québec, Canada,* H3A 2T8
[2] *LMM (CNRS-URA 229) Boite* 162, *Université Pierre et Marie Curie,* 4 *Place Jussieu, Paris* 75252 *Cedex* 05, *France*
[3] *Mathematical Sciences, Clemsen University,* Box 341907, *Clemsen, SC* 29634–1907, *USA*

Accepted 2000 September 29. Received 2000 September 29; in original form 1997 July 22

SUMMARY

Scaling models of geofields attempt to capture the strong and wide-range variability ubiquitous in geosystems. Unfortunately, they are generally both isotropic (self-similar) and monofractal (non-intermittent, quasi-Gaussian). In this first paper of a two-paper series, we lift the first of these restrictions, arguing that anisotropic scaling is essential for taking into account the stratification of the Earth and its consequences. In particular, at scales below several thousand kilometres we model the thin or Curie-depth-limited crustal magnetization and the corresponding surface magnetic field (**B**) by using anisotropic scaling. We show that it generically gives rise to a new intermediate scaling ('red noise') surface **B** field regime quantitatively very close to that observed on two sets of regional surface **B** field surveys. This scaling is impossible to explain using standard self-similar models. Using these data as well as horizontal and vertical susceptibility data, we estimate the basic model parameters and show that that model is compatible with the available data. In Paper II we lift the monofractal restriction and perform multifractal analyses; we then extend the anisotropic scaling model to include multifractal **B** and magnetization fields.

Key words: anisotropic scaling, geomagnetism, multifractal analyses.

1 INTRODUCTION

1.1 An anisotropic multiscaling framework

To a first approximation, the Earth's magnetic field is that of an effective dipole source at the Earth's centre superposed on a field (partially induced by the latter) originating in the magnetized crust. Compared to the crust, the mantle is generally below the Curie depth (it is too hot to be magnetized) while simultaneously being viscous (hence of low velocity) and of low electrical conductivity. It is therefore not believed to provide a significant source or sink for the magnetic field. Since there is a rapid fall-off in the contribution from a given Fourier component of the source with depth, the (distant) core only contributes very low-wavenumber variability (wavelengths of thousands of kilometres); all the higher frequencies are presumed to come from a thin layer in the crust (Lowes 1974 estimated that the core dominates for spherical harmonics $<$order 11). This picture might lead to the naive expectation that there would be little spectral energy in the horizontal surface magnetic field between scales corresponding to the Curie depth ($\approx$10–100 km) and several thousand kilometres. However, various regional studies (especially over oceans, e.g. Harrison & Carle 1981; Harrison *et al.* 1986; Counil *et al.* 1989) have found on the contrary significant ('red noise'-type) spectral energy in this scale region. [Following Wasilewski & Mayhew (1992), Maus *et al.* 1997 made a distinction between the Curie depth and the more general term 'depth to the bottom' (DTB), which takes into account the possibility that due to the presence of (mantle-type) ultramafic rocks with very low magnetizations the magnetization may approach zero even at temperatures below the Curie temperature. Here we use the expression 'Curie depth' to be synonymous with DTB.]

The main challenge in statistically modelling these 'intermediate-scale anomalies' in the magnetization is that in order to yield the 'red noise' spectrum, the model must have long-range correlations in the horizontal while simultaneously taking into account the vertical structure. The magnetization—which includes the obvious stratification of the Earth—is characterized by sudden transitions (occasional large gradients) and the existence of easily identifiable strata. The obvious geophysical models with these properties are the scaling models, in particular the (anisotropic) multifractal models, which can be both stratified and involve strong structures (sharp gradients, 'singularities') at all scales (see Lovejoy & Schertzer 1995 and Pecknold *et al.* 1997b for reviews). Indeed, due to the ubiquity of fractal structures and multifractal statistics, and to the existence of stable, attractive multifractal processes, Schertzer

GJI 72960-8 10/1/01 13:12:29 Rev 6.05e/W (Mar 29 1999)
The Charlesworth Group, Huddersfield 01484 517077

& Lovejoy (1991) and Lovejoy & Schertzer (1998, 1999) have argued that anisotropic multifractals can provide a unifying framework for geophysics. The relevance of scaling models to solid Earth geophysics has probably been most clearly demonstrated in topography from planetary scales to 90 m or less (see e.g. Venig-Meinesz 1951; Bell 1975; Bills & Kobrick 1985; Klinkenberg & Clarke 1992; Lovejoy & Schertzer 1990; Lavallée *et al.* 1993; Weissel & Pratson 1994; Lovejoy *et al.* 1995; Pecknold *et al.* 1997b, 2000).

Direct evidence for the scaling of the crust magnetization is quite limited, the primary references being the analyses of the horizontal and vertical susceptibilities by Pilkington & Todoeschuk (1993, 1995) (as discussed below these are magnetization surrogates). However, many other geophysical fields and processes that are statistically related to magnetization (notably seismic velocities, gamma emission, rock density) are known to be scaling (see especially Pilkington & Todoeschuk 1993, 1995; Turcotte 1989; Leary 1997; Shiomi *et al.* 1997; Marsan & Bean 1999). It is therefore natural to hypothesize that crustal magnetization is scale-invariant over wide ranges in scale; this hypothesis in various forms—including the link between scaling magnetization and surface magnetic fields—has indeed already been considered by several authors. In particular, Gregotski *et al.* (1991), Pilkington & Todoeschuk (1993, 1995), Pilkington *et al.* (1994), Maus & Dimri (1995, 1996), Maus *et al.* (1997) and Zhou & Thybo (1998) assumed generally non-trivial scaling (fractal) magnetization fields, whereas Fedi *et al.* (1997) used white noise ('trivial' scaling) source distributions.

These pioneering attempts to place the relation between volume magnetization and (crustal) surface magnetic fields into a statistical scaling framework represent a major advance. Several of them (especially Pilkington *et al.* 1994 and Maus *et al.* 1997) go well beyond attempts to refine Spector & Grant (1970) type one-to-one (deterministic) relations between spectral magnetic anomalies and spatially localized magnetization sources; they have made first steps towards an understanding of the overall *statistical* relations between the fields. Unfortunately, they have generally shared two simplistic assumptions that have hampered progress. The first is the restriction to scaling isotropy (equivalently, 'self-similarity'); the second is the restriction to fractal geometry in which the statistics are described by a single scaling exponent such as the fractal dimension or—in this case equivalently—the spectral exponent. [Note that the use of spectral analysis for estimating fractal dimensions is only valid for monofractal systems. Neglect of this fact has led to sterile debates about the value of supposedly unique fractal dimensions; see the discussion in Lavallée *et al.* (1993).]

The main purpose of this series of papers is to show that the two missing ingredients—anisotropy and multifractality—are indispensable for realistic models (including numerical simulations) of magnetization and magnetic field. In Paper I of this two-paper series, we focus on the issue of anisotropic scaling, showing that—even at the level of power spectra (which are simply second-order statistics)—anisotropy is fundamental to an understanding of the most basic spectral scaling properties of the magnetic field. However, unless the fields are quasi-Gaussian (hence non-intermittent, lacking in strong structures and significant anomalies) the spectrum does not adequately characterize the processes; it gives only limited statistical information (we exclude here the essentially *multifractal* analysis technique, which consists of systematically determining all the spectral exponents of all the powers of the fields). Starting in the early 1980s, it has been increasingly recognized that a full statistical characterization of a scaling field is a *multi* not a *mono*fractal one. In Paper II, we give such a multifractal characterization of the magnetic field. This, combined with the stratification (quantified in Paper I) enables us to construct explicit multifractal simulations—which by allowing comparison between the simulated and empirical magnetic field and magnetization statistics can be used to test the scaling assumptions. Both of these papers are developments of work described in the PhD thesis of Pecknold (2000).

1.2 Outline of Paper I

In Paper I we use magnetic survey data from two different regions in Canada involving, respectively, seven and five regional magnetic surveys at about 800 m resolution. In addition, we use two borehole (vertical) and two surface *in situ* (horizontal) susceptibility spectra. By studying purely second-order statistics (which are theoretically convenient), the goal is to establish the anisotropy of the spectral scaling of the magnetization and show that this is quantitatively compatible with the observed magnetic field spectra (including spectral breaks). Even at the level of spectra, the theory involves two basic exponents (H_z, s) from which we theoretically derive four spectral exponents (those of the horizontal and vertical magnetizations and of the high- and intermediate-wavenumber surface magnetic fields). The reasonable fit of the four empirical exponents with those predicted from a single (H_z, s) pair is therefore a fairly stringent test of the theory.

In Section 2 the basic data are described and in Section 3 we give a recap of the basic (classical) potential theory relating magnetization and magnetic field (nearly the same geopotential theory relates rock density and the gravity field). In Section 4 we outline the theory of scaling anisotropy (GSI) and in Section 5 we propose a simple spectral model for the magnetization that incorporates scaling anisotropy. In Section 6 we compare magnetic susceptibility data and surface magnetic field data with the predictions of the model and in Section 7 we conclude. Appendix A gives some mathematical details for the spectral model while Appendix B shows the effect of scaling horizontal anisotropy on the usual (isotropic) power spectrum.

2 THE MAGNETIC FIELD SURVEYS AND THEIR SPECTRAL CHARACTERISTICS

The interpretation of aeromagnetic data is complicated notably since the magnetic field of the Earth is a superposition of the main (internal) field of the planet, of fields arising from electrical currents flowing in the ionized upper atmosphere, and of fields induced by currents flowing within the Earth. However, sophisticated analysis techniques are available, yielding surveys of the total magnetic field anomalies ($\mathbf{B}_{\text{observed}} - \bar{\mathbf{B}}$), downward continued to ground level ($\bar{\mathbf{B}}$ is a constant regional average). The downward continuation error is small; it presumably leads to a white noise flattening of the spectra accounting, for example, for the high-wavenumber curvature in data set #2 (see Fig. 1). The surveys most extensively used here were the seven aeromagnetic surveys (taken with 300 m of mean

GJI 72960-8 10/1/01 13:13:04 Rev 6.05e/W (Mar 29 1999)
The Charlesworth Group, Huddersfield 01484 517077

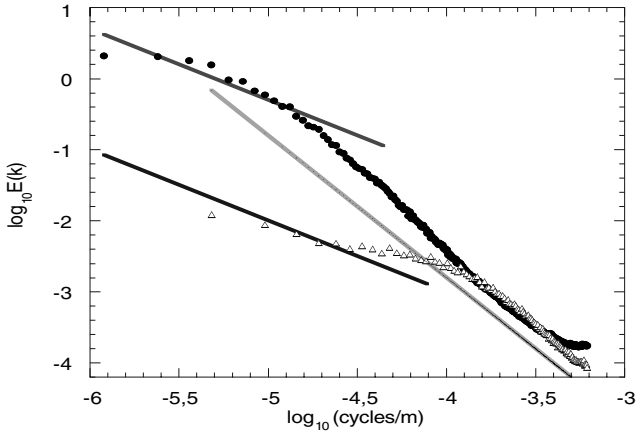

33 **Figure 1.** Power spectra of aeromagnetic anomaly fields from data set #1, 2 regional surveys, shown as triangles and circles, respectively. Superimposed for reference are line segments with the theoretical high- and low-wavenumber slopes, $\beta_h = 2$ and $\beta_i = 1$ (see Section 6). The spectra have been normalized so that the high-wavenumber regions roughly coincide.

terrain clearance) from eastern Canada indicated in Table 1, with a grid spacing of 812.8 m at the survey altitude. The fields on 256×256 pixel square grids were analysed for both their power spectra (Paper I) and their multifractal parameters (Paper II). In addition to this 'data set #1', M. Pilkington also kindly provided us with the spectra of each of five other regional surveys (also eastern Canada, but generally more northern) ('data set #2') described in Pilkington & Todeschuck (1993) (at the same spatial resolution but each with 512×512 pixels). All data sets were taken from the Canadian shield.

Spectral analysis is one of the oldest and most familiar techniques for analysing scaling; it is indeed quite sensitive to scaling limits and in addition it gives us a useful spectral exponent. Since it is also theoretically convenient, especially in geopotential problems, we will use it throughout Paper I; a full statistical characterization of the fields (involving moments of all orders) is discussed in Paper II. In Fig. 1, we show the isotropic power spectrum $E(k)$ of the two data sets (where $\mathbf{k}$ is the wave vector, $k = |\mathbf{k}|$). $E(k)$ is defined as the ensemble average of the square of the modulus of the Fourier transform of the data set integrated over all angles in Fourier space. For isotropic scale invariance, $E(k)$ is a power law,

$$E(k) \sim k^{-\beta}, \tag{1}$$

where β is the spectral exponent. This definition, used in turbulence, has the advantage that for isotropic processes, the exponent is the same in all subspaces (e.g. a 1-D spectrum of an isotropic 3-D process defined this way is the same as the 3-D spectrum). It is generally different from the angle-averaged spectral power density. For example, in two dimensions there is an extra factor $2\pi k$ so that $\beta = -\alpha - 1$, where α is the angle-averaged exponent used in Pilkington & Todoeschuk (1995). With this definition, in d dimensions, Gaussian white noise thus has $E(k) \approx k^{d-1}$. As a final comment, we mention that Maus *et al.* (1997) advocated a slightly different definition of the power spectrum: the angular average of the log of the spectral density. However, this is not the same as the standard definition used here, and at least for multifractal processes, the relation between the two is not known.

Table 1. Location of data set #1. In all cases, resolution was 812.8 m.

Data set	Longitude	Latitude
east	87	50
west	87	50
meg3	66	49
nm151	94	49
nn151	94	53
nn151	100	57
no141	100	53

As can be seen from the power spectra of both data sets (Fig. 1), a break in the scaling occurs at about 10 and 80 km in the data sets #1 and #2, respectively. We see below that it is likely to be a horizontal manifestation of somewhat deeper Curie depths (approximately 20–30 km and 80–100 km, respectively; see, however, Appendix B). This agrees roughly with estimates obtained from typical values of the Curie temperature of 800–900 K and vertical thermal gradients of 20 $K\ \mathrm{km}^{-1}$ (see e.g. Stacey 1992). These estimates yield a depth of approximately 30 km. With the help of an isotropic spectral model, Maus *et al.* (1997) found values of Curie depth in the range 10–50 km for South African and Central Asian surveys. Since the exact estimates depend somewhat on the spectral assumptions, their (isotropic) values are compatible with our (anisotropic) values. Also shown for future reference are high- and low-wavenumber reference lines, with values $\beta_h = 2$ and $\beta_i = 1$ (whose values we explain below by the combined effects of scaling stratification and Curie depth). For comparison, using their isotropic model, Maus *et al.* (1997) found spectral exponents corresponding to β_h in the range 1.5–2 (their parameter $s = \beta_h + 2$ is in the range 3.5–4), that is, essentially the same as the high-wavenumber regime values found here (we will see that the anisotropy does not affect the high-wavenumber exponent β_h).

Finally, in Figs 2 and 3 the spectra from these regional surveys are compared to the very low-wavenumber (Magsat) results of Langel & Estes (1982), which also shows how our model of the crust magnetization (discussed in Section 5) can account well for the entire large-wavenumber part of the spectrum. From the latter, we see that the very low-wavenumber core region gives way to a flatter intermediate region at spherical harmonics $n \approx 20$ corresponding to wavenumbers $20/40\,000\ \mathrm{km}^{-1} = (2000\ \mathrm{km})^{-1}$. This flattening suggests that the surface **B** field has contributions from the crustal magnetization at wavenumbers at least this low, hence the intermediate scaling regime described here has a lower bound $k_{ic} < (2000\ \mathrm{km})^{-1}$. As can be seen from the numerical simulation in Figs 2 and 3, this is relatively easy to achieve using realistic magnetization parameters (as long as the stratification is appropriately taken into account). 7

3 CLASSICAL THEORY RELATING M AND SURFACE B STATISTICS

Before considering the measurement of anisotropy in the horizontal plane, we first wish to determine the possible effects of anisotropy in the vertical plane as well as the effects of a low-wavenumber cut-off such as the Curie depth. We start with the convolution formula for the scalar magnetic potential $V(\mathbf{r})$ due

GJI 72960-8 10/1/01 13:13:04 Rev 6.05e/W (Mar 29 1999)
The Charlesworth Group, Huddersfield 01484 517077

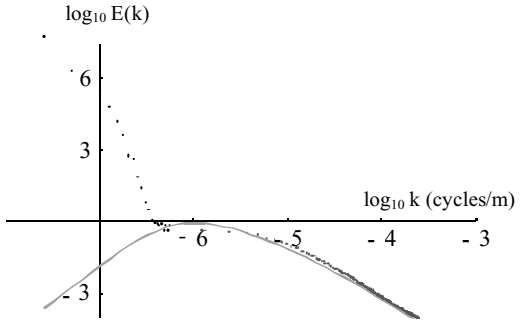

Figure 2. Theoretical and experimental energy spectra of surface magnetic fields. The high-wavenumber data points are from data set #2 while the low-wavenumber points are from the global (Magsat) Langel & Estes (1982) spherical harmonics ($n=1$ was taken as 40 000 km^{-1}). Also shown is the theory (smooth curve calculated with parameters $H_z=2$, $k_s=10^{-7.6}$ m^{-1}; spheroscale $\approx$ size of the Earth; $s=4.4$, $k_c=10^{-5}$ m^{-1}; Curie depth approximately 100 km; see Section 6). These parameters imply $\beta_x=s-H_z-1=1.4$, $\beta_z=1.2$ for the magnetization, which are close to those found. The lower limit to the intermediate range (eq. 22b) is approximately (2000 km)$^{-1}$. The theory is adjusted up and down for superposition, i.e. $E(k)$ is in arbitrary units.

34

to a magnetization density $\mathbf{M}(\mathbf{r})$,

$$V(\mathbf{r}) = C_M \int \mathbf{M}(\mathbf{r}') \cdot \nabla \frac{1}{|\mathbf{r}-\mathbf{r}'|}\, d\mathbf{r}', \quad (2)$$

where $C_M=\mu_0/4\pi$ in SI units, equal to 1 in cgs units (since we are interested only in the scaling, we set $C_M=1$). The scalar magnetic potential exists whenever $\nabla\times\mathbf{B}=0$, i.e. in a non-magnetic material, where there are no currents (air is a good approximation to this). We can then calculate the total field anomaly, which is considered to be the component of $\mathbf{B}$ along the direction of the (roughly constant) regional mean $\hat{f}$,

$$\hat{f}\cdot\mathbf{B} = -\hat{f}\cdot\nabla V. \quad (3)$$

Adapting a standard result (see e.g. Blakely 1995), we have the following contribution to the horizontal Fourier transform of the surface field due to the magnetization at depth z of a layer of thickness dz:

$$d\mathbf{B}(K,\theta) = [f_z + iF\cos(\theta-\theta_F)][M_z(K,\theta,z) + iM(K,\theta,z)\cos(\theta-\theta_M)]Ke^{-Kz}dz, \quad z\geq 0, \quad (4a)$$

where K, θ are the horizontal polar Fourier coordinates, θ_F, θ_M are the horizontal polar angles of $\mathbf{M}$ and $\hat{f}$, and $F^2=f_x^2+f_y^2$, $K^2=k_x^2+k_y^2$ and $M^2=M_x^2+M_y^2$, with $\mathbf{M}(K,\theta,z)$ the horizontal Fourier transform of the magnetization layer at depth z and $d\mathbf{B}(K,\theta)$ the infinitesimal contribution to the transform of the magnetic field at the *surface* ($z=0$) due to the layer at depth z, thickness dz. The main simplifying choices are those about $\mathbf{M}$. Naidu (1968) took an example where the cross-correlations between the components of $\mathbf{M}$ were zero and $P_{M_z}=P_{M_x}=P_{M_y}$ [P is a spectral density, e.g. $P_{M_z}(\mathbf{k})=\langle|M_z(\mathbf{k})|^2\rangle$, where $M_z(\mathbf{k})$ is the Fourier transform of the z-component of $\mathbf{M}$], whereas Pilkington & Todeschuck (1995) assumed that $\mathbf{M}$ has a constant direction throughout, and only the magnitude varies with position. This constant direction approximation corresponds to the case where $\mathbf{M}$ is entirely induced by the Earth's field, with the latter being roughly constant over the region of interest. This is probably a reasonable approximation for the $\mathbf{B}$ field in the limited regions studied here. For our purposes, we will therefore assume that $\mathbf{M}$ only has a z-component and also take anomalies in the z direction ($\hat{f}=f_z\hat{z}$; the survey regions were in fact not too far from the magnetic North Pole). Since the critical factor [$K^2/(K^2+k_x^2)$; see below] is the same for all the terms, the scaling results will probably not be sensitive to this choice.

With these simplifications in eq. (4a), we obtain

$$dB_z(K,\theta) = M_z(K,\theta,z)Ke^{-Kz}dz. \quad (4b)$$

Due to the exponential fall-off (and since Spector & Grant 1970), this formula has been widely used as the basis for interpreting horizontal $\mathbf{B}$ anomalies in terms of depths to sources. In Appendix A, we derive a statistical variant of this interpretation (valid only for distances smaller than the Curie depth).

If we now express M_z in terms of its Fourier transform,

$$M_z(k_x,k_y,z) = \int_{-\infty}^{\infty} e^{ik_z z} M_z(k_x,k_y,k_z)dk_z. \quad (5)$$

We can then insert this into eq. (4b) with $\hat{f}\cdot\mathbf{B}=B_z$ and integrate the result over z. We obtain (Naidu 1968)

$$B_z(K,\theta) = \int_{-\infty}^{\infty} M_z(K,\theta,k_z)\frac{Kdk_z}{K+ik_z}. \quad (6)$$

This is the equation we use in Paper II for simulating B_z given M_z. It is now straightforward to determine the relationship between the spectral density of B_z and M_z; we merely multiply the above by $B_z^*(K',\theta')$ (where the asterisk represents the complex conjugate) and take ensemble averages using the fact that M_z is assumed statistically translationally invariant for $z<0$. We thereby obtain the standard result (Naidu 1968)

$$P_{B_z}(K,\theta) = \int \frac{K^2}{K^2+k_z^2}\langle|M_z(K,\theta,k_z)|^2\rangle dk_z = \int \frac{K^2}{K^2+k_z^2} P_{M_z}(K,\theta,k_z)dk_z, \quad (7)$$

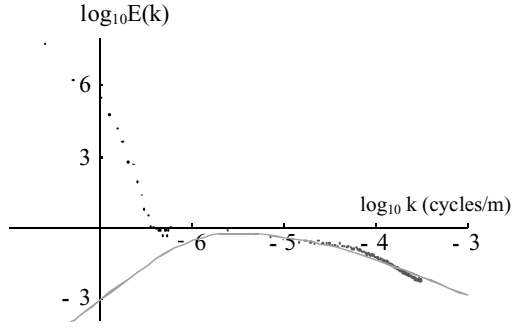

Figure 3. Theoretical and experimental energy spectra of surface magnetic fields. The high-wavenumber data points are from data set #1 while the low-wavenumber points are from the global (Magsat) Langel & Estes (1982) spherical harmonics ($n=1$ was taken as 40 000 km^{-1}). Also shown is the theory [smooth curve calculated with parameters $H_z=2$, $k_s=10^{-7.6}$ m^{-1}; spheroscale $\approx$ size of the Earth; $s=3.6$, $k_c=10^{-4.5}$ m^{-1}; i.e. Curie depth $\approx$30 km, hence $k_{ic}\approx$(1000 km)$^{-1}$]). The result is not very sensitive to the values of k_s, H_z. $E(k)$ is again in arbitrary units.

35

GJI 72960-8 10/1/01 13:13:05 Rev 6.05e/W (Mar 29 1999)
The Charlesworth Group, Huddersfield 01484 517077

where we have expressed the 2-D horizontal spectral density of the surface magnetic field (P_{B_z}) in terms of the 3-D spectral density of the magnetization (P_{M_z}).

8 Dropping (here and below) explicit reference to the z-component, assuming that **B** is horizontally isotropic [i.e. $P_B(K, \theta) = P_B(K)$], then the isotropic *horizontal* spectrum of **B** at $z = 0$ is thus

$$E_B(K) = \int_0^{2\pi} K P_B(K) d\theta = 2\pi K P_B(K); \quad (8)$$

the spectral exponents of $E(K)$ and $P(K)$ and the latter thus differ by 1. Note that in the following we will once again ignore constant factors since we are interested in the scaling.

4 ANISOTROPY AND GENERALIZED SCALE INVARIANCE

4.1 The GSI framework

Although the anisotropy of the Earth in the vertical plane is quite evident, the horizontal plane also displays strong scale-dependent anisotropy. Perhaps the most obvious example of the latter is that associated with the mid-ocean ridges, which display large-scale structures oriented roughly perpendicular to the small-scale ridges. Another example of anisotropy is the

9 atmosphere, whose stratification of the vertical with respect to the horizontal gives it an elliptical dimension of $23/9 = 2.55\ldots$ rather than the spatial dimension 3 (see Lazarev *et al.* 1994 for recent work). Until recently, scaling models and analyses have avoided dealing with such anisotropy because scale invariance has traditionally been associated with self-similarity—and conversely, an absence of self-similarity has been associated with characteristic scales/breaks in the scaling. However, with the advent of the general formalism for scale invariance, generalized scale invariance or GSI (Schertzer & Lovejoy 1985a), this identification is quite outdated because isotropic scaling is neither expected nor required. In fact, the use of isotropic scaling statistics such as the usual energy spectrum will generally lead to spurious scaling breaks if anisotropies are present (see Appendix B). On the other hand, the presence of anomalous scale breaks in the energy spectrum of a field can, as we see in the case of the magnetic data, be evidence of the presence of anisotropy in the underlying source, in this case the crust's magnetization. In a recent paper, Lovejoy *et al.* (2000) have shown how very similar anisotropic scaling in the closely analogous potential problem of rock density can explain the medium- and high-wavenumber surface gravity statistics. The

10 assumption of isotropy is often made implicitly, and if justified at all is done so by its theoretical simplicity. The assumption is all the more pervasive since the anisotropic nature of most geophysical systems is usually hidden through the use of isotropic analysis techniques. Nevertheless, as we show below (see Paper II for analyses and models of horizontal anisotropy), these anisotropies do play an important part in determining the texture and morphology of the fields.

Outside the GSI framework, with the exception of the special case of self-affinity, there have been only a few attempts to deal with scaling anisotropy. The most common approach is the *ad hoc* introduction of scaling exponents varying as functions of direction. This method of handling scaling anisotropy has been independently proposed by several authors (Fox & Hayes 1985; Van Zandt *et al.* 1990; Pilkington & Todoeschuk 1993). Although at first sight this is appealing, it turns out to be incompatible with scaling—it necessarily involves absolute, rather than relative, notions of scale: any underlying dynamics will be fundamentally scale-dependent, rather than independent of size.

To develop the framework of GSI, we need several components. The first, most basic of these is the scale-changing operator, T_λ. Since scale invariance demands that the statistical properties only depend on the scale ratio λ and not actual sizes. 11 This implies that a scale change λ_1 followed by λ_2 must be equivalent to a single change of $\lambda = \lambda_1\lambda_2$, i.e. $T_\lambda = T_{\lambda 1} T_{\lambda 2} = T_{\lambda 2} T_{\lambda 1}$ if and only if $\lambda = \lambda_1\lambda_2$. T_λ must therefore have group properties; in particular it admits a generator **G** such that

$$T_\lambda = \lambda^{\mathbf{G}}. \quad (9)$$

[A linear GSI system can be defined either in Fourier space or in real space, the only differences being the sign in the exponent and the fact that the real space generator is the adjoint (matrix transpose here) of the Fourier space generator.]

The second element is a reference (unit) ball (B_1) whose boundary defines the unit vectors; T_λ generates all the other balls by enlargements of B_1: $B_\lambda = T_\lambda B_1$. They need merely define a series of strictly increasing balls, i.e. if $B_\lambda = T_\lambda B_1$ then $\lambda' > \lambda \Rightarrow B_\lambda \subset B_{\lambda'} \ldots$. A final element is a definition of the measure of each of the elementary balls; these elementary measures can then be used to define the measures of arbitrary sets of points in the usual way (yielding for example anisotropic Hausdorff measures and dimensions; this is described in detail 12 in Schertzer & Lovejoy 1985b). In the anisotropic case, if a scale exists at which the system is isotropic, we call this scale the *spheroscale* (more generally, even if there is no scale of perfect isotropy, there will generally be a scale where the sizes of structures in the horizontal and vertical directions are the same); use of this ball to define the unit scale is quite convenient.

In the case of linear GSI, **G** is a matrix; the λ factor enlargement of a vector $\mathbf{k}_1 = (k_{x1}, k_{y1}, k_{z1})$ (for the 3-D Fourier space used below) is thus given by $\mathbf{k}_\lambda = \lambda^{\mathbf{G}} \mathbf{k}_1$; the exponentiation of **G** can be performed using a series expansion. When **G** is the identity matrix we have the isotropic case and when **G** is diagonal, the standard self-affine case. When **G** has off-diagonal elements, structures will generally change orientation with scale.

4.2 Anisotropy in the horizontal plane: differential rotation

For simplicity, we consider the case where the overall stratification is perpendicular to gravity. In 3-D linear GSI, this implies a matrix

$$\mathbf{G} = \begin{pmatrix} \mathbf{G}_h & 0 \\ 0 & H_z \end{pmatrix}, \quad (10a)$$

where $\mathbf{G}_h$ is a 2×2 matrix (generating the horizontal anisotropy). The off-diagonal elements indicated by zeroes are a simplification that disallows rotation of structures in the vertical plane. H_z then characterizes the degree of this stratification in the vertical plane.

Let us first consider the simpler (2-D) $\mathbf{G}_h$ that acts only in the horizontal plane. We may decompose $\mathbf{G}_h$ into pseudo-quaternion generators (Schertzer & Lovejoy 1985b; Lovejoy &

GJI 72960-8 10/1/01 13:13:06 Rev 6.05e/W (Mar 29 1999)
The Charlesworth Group, Huddersfield 01484 517077

Schertzer 1985),

$$\mathbf{G}_{\rm h} = d\mathbf{1} + e\mathbf{I} + f\mathbf{J} + c\mathbf{K}\,, \tag{10b}$$

where

$$\mathbf{1} = \begin{pmatrix} 1 & 0 \\ 0 & 1 \end{pmatrix}, \quad \mathbf{I} = \begin{pmatrix} 0 & -1 \\ 1 & 0 \end{pmatrix}, \quad \mathbf{J} = \begin{pmatrix} 0 & 1 \\ 1 & 0 \end{pmatrix}, \quad \mathbf{K} = \begin{pmatrix} 1 & 0 \\ 0 & -1 \end{pmatrix}. \tag{10c}$$

A fundamental parameter for the description of the overall type of anisotropy present in the system will be given by the eigenvalues ($\pm a$) of the traceless part of $\mathbf{G}_{\rm h}$,

$$a^2 = c^2 + f^2 - e^2\,. \tag{11}$$

In the case where $a^2 < 0$, we say that the system is rotation-dominant: as the scale changes, the balls rotate through an infinite angle of rotation (although for a finite total scale ratio, only a finite amount of rotation is possible). If $a^2 > 0$ we call the system stratification-dominant: in a similar manner, an indefinitely large 'stretching' of the unit ball occurs, but the total amount of rotation never exceeds $\pi/2$. Note that in the case where a spheroscale exists, all the balls are ellipses, and the strictly increasing (non-crossing) condition mentioned above required to guarantee uniqueness reduces to $d^2 > c^2 + f^2$.

An analysis of the anisotropies of our system thus involves determining the parameters c, d, f and e, along with the unit ball. This completely determines the scaling anisotropy in linear GSI. For cases involving position-dependent anisotropy, non-linear GSI must be used (see e.g. a simple non-linear GSI model of the stratification of rock density in Lovejoy & Schertzer 1999) or alternatively the linear GSI approximation may be made over subregions of the system.

13

We now turn our attention to the full 3-D vertically stratified generator $\mathbf{G}$ (eq. 10a). A convenient measure of the overall stratification is given by the 'elliptical' dimension, $d_{\rm el}$, defined as

$$d_{\rm el} = {\rm Trace}(\mathbf{G})\,. \tag{12}$$

$d_{\rm el}$ quantifies the rate at which the volume ('vol') of the balls changes with scale: ${\rm vol}(B_\lambda) = \lambda^{d_{\rm el}}{\rm vol}(B_1)$. With the above (eqs 10a and b) 3×3 matrix for $\mathbf{G}$, we have $d_{\rm el} = 2d + H_z$. Assuming that there is no overall stratification in the horizontal plane, ${\rm Trace}(\mathbf{G}_{\rm h}) = 2$ so that $d = 1$ in eq. (10b) and $d_{\rm el} = 2 + H_z$. H_z thus characterizes the overall degree of stratification, with $H_z = 1$ corresponding to isotropy (in three dimensions) and $H_z = 0$ to completely flat 2-D structures. If $H_z < 1$, the horizontal stratification becomes stronger and stronger at larger scales (this is the case of the atmosphere, where $H_z \approx 5/9$; see Schertzer & Lovejoy 1985a; Lazarev *et al.* 1994). When $H_z > 1$ (as is found here), then instead the horizontal stratification becomes stronger at the smaller scales. Recently, Lovejoy *et al.* (2000) has shown theoretically that $H_z = 3$ in the temperature, velocity and density field in mantle convection. In this case, it may be advantageous to use the fact that a GSI system is non-unique; in particular, we may choose to measure scale by the vertical (rather than horizontal) extent of a structure; this is equivalent to using the following new (primed) scale ratios and generators:

$$\lambda' = \lambda^{H_z}\,, \tag{13a}$$

$$\mathbf{G}' = \begin{pmatrix} \mathbf{G}_h/H_z & 0 \\ 0 & 1 \end{pmatrix}, \tag{13b}$$

which clearly defines the same GSI system since $T_{\lambda'} = \lambda'^{\mathbf{G}'} = T_\lambda$. With this choice (which is equivalent to using the vertical rather than the horizontal extent of structures to measure their scale), we have $d'_{\rm el} = {\rm Trace}\,\mathbf{G}' = 2/H_z + 1$, hence for $H_z \geq 1$, $2 \leq d'_{\rm el} \leq 3$, which restores the intuitive interpretation of $d_{\rm el}$ as quantifying the stratification between the isotropic 2- and 3-D limits. In this paper, we retain the horizontal size of a structure as the definition of scale, finding empirically that $d_{\rm el} > 3$.

5 A SIMPLE SPECTRAL MODEL WITH VERTICAL STRATIFICATION ONLY

In this section, we present a spectral model that is symmetric with respect to generalized scale changes. Non-dimensional spectral densities $P(\mathbf{k})$ respecting GSI satisfy

$$P(T_\lambda \mathbf{k}) = \lambda^{-s} P(\mathbf{k})\,, \tag{14}$$

where s is a scaling exponent; determination of the full GSI system involves the determination of $\mathbf{G}$ (or at least a linear approximation to $\mathbf{G}$ as here) as well as s. The spectral density P can be non-dimensionalized by using the dimensional spectral density at a convenient reference wavenumber; below, this will be taken as the spheroscale. In order to understand (and solve) this equation, it is helpful to introduce the 'scale function' $\|(\mathbf{K}, k_z)\|$ (Marsan *et al.* 1996; Pecknold *et al.* 1997a). The scale function tells us how much we must zoom in (or out) of a unit vector (i.e. from the boundary of the unit ball) in order to reach the vector $\mathbf{k} = (\mathbf{K}, k_z)$. If $\mathbf{k}_1 = (\mathbf{K}_1, k_{z,1})$ is a unit vector (i.e. $\mathbf{k}_1 \in \partial B_1$, where ∂B_1 is the boundary of the unit ball B_1), then by definition

14

$$\|(\mathbf{K}_1, k_{z,1})\| = 1\,. \tag{15a}$$

The scale function for other vectors is defined by

$$\|(\mathbf{K}, k_z)\| = \lambda \Leftrightarrow (\mathbf{K}, k_z) = T_\lambda(\mathbf{K}_1, k_{k,1})\,. \tag{15b}$$

From this definition, we see that for all vectors and all scale ratios λ', the scale function satisfies

$$\|T_{\lambda'}(\mathbf{K}, k_z)\| = \lambda' \|(\mathbf{K}, k_z)\|\,. \tag{15c}$$

The scale function is analogous to a norm, but need not respect the triangle inequality (it needs merely to define a series of decreasing balls, i.e. if $B_\lambda = T_\lambda B_1$ then $\lambda' > \lambda \Rightarrow B_{\lambda'} \subset B_\lambda$). For a vector $(\mathbf{K}, k_z)$, the corresponding λ is the ratio of the spheroscale to the scale of $\|(\mathbf{K}, k_z)\|$. With the scale function, eq. (14) is satisfied for

$$P(\mathbf{K}, k_z) = \|(\mathbf{K}, k_z)\|^{-s}\,. \tag{16a}$$

Equivalently—as recently advocated by Maus (1999)—we can express the statistics in real space. To do this, first define the qth-order anisotropic structure function,

$$\langle |\Delta M(\Delta\mathbf{r})|^q \rangle = \|\Delta\mathbf{r}\|^{\xi(q)}\,; \qquad \Delta M(\Delta\mathbf{r}) = M(\mathbf{r} + \Delta\mathbf{r}) - M(\mathbf{r})\,, \tag{16b}$$

GJI 72960-8 10/1/01 13:13:07 Rev 6.05e/W (Mar 29 1999)
The Charlesworth Group, Huddersfield 01484 517077

where $\Delta\mathbf{r}=(\Delta x, \Delta y, \Delta z)$ and M is a non-dimensional magnetization vector component. Due to the (generalized, anisotropic) Tauberian theorem relating real space and Fourier space scaling (Pflug *et al*. 1991), when $q=2$ the spectral scaling (eq. 16a) corresponds to the real space variogramme/structure function statistics (eq. 16b) with exponent

$$\xi(2) = s - d_{\rm el}\,. \tag{16c}$$

To consider only the effect of vertical stratification, we restrict ourselves to a spectral density P that is symmetric with respect to the generator,

$$\mathbf{G} = \begin{pmatrix} 1 & 0 & 0 \\ 0 & 1 & 0 \\ 0 & 0 & H_z \end{pmatrix} \tag{17}$$

(i.e. it satisfies eq. 14 for P with this generator). A convenient, but not unique, choice of $\|(\mathbf{K}, k_z)\|$ compatible with the linear generator given in eq. (17) is

$$\|(\mathbf{K}, k_z)\| = \left[\left(\frac{K}{k_{\rm s}}\right)^2 + \left(\frac{k_z}{k_{\rm s}}\right)^{2/H_z}\right]^{1/2}, \tag{18}$$

where as above $\boldsymbol{K}=(k_x, k_y)$ and we have introduced a 'spheroscale' at corresponding wavenumber $k_{\rm s}$. At the spheroscale, $P(k_{\rm s}, 0, 0)=P(0, k_{\rm s}, 0)=P(0, 0, k_{\rm s})=1$, i.e. P is roughly constant over a sphere (horizontal and vertical fluctuations have the same variance, $\|(k_{\rm s}, 0, 0)\|=\|(0, k_{\rm s}, 0)\|=\|(0, 0, k_{\rm s})\|=1$); this corresponds to non-dimensionalizing P using the value at the spheroscale. Other choices of $\|(\mathbf{K}, k_z)\|$ that are symmetric with respect to the generator in eq. (17) correspond to changing the unit ball. Since we are only interested in the resulting scaling (of the power spectrum), this is not too important.

Let us now take the spectral density defined by eqs (16) and (18) as a model for the M spectrum,

$$P_{\rm M}(\mathbf{K}, k_z) = \|(\mathbf{K}, k_z)\|^{-s} = \left[\left(\frac{K}{k_{\rm s}}\right)^2 + \left(\frac{k_z}{k_{\rm s}}\right)^{2/H_z}\right]^{-s/2}, \tag{19}$$

Fig. 4 shows an example of the typical real space structures implied by such a spectrum (that is, those that give the dominant contribution to the second-order statistical moment; the structures are those of the isolines of the second-order structure function; see eq. 16b). We now note that the 1-D horizontal and 1-D vertical spectra [obtained by integrating $P_{\rm M}$ given by eq. (19) over, respectively, the vertical and horizontal wavenumbers] are each (scaling) power laws with the horizontal spectrum

$$E_{\rm M}(K) \approx k_{\rm s}^2 \left(\frac{K}{k_{\rm s}}\right)^{-\beta_x}; \quad \beta_x = (s - H_z - 1) \quad (\text{if } s > H_z) \tag{20a}$$

(if $s<H_z$ then there is a high-frequency divergence; for finite high-wavenumber cut-off, $\beta_x=-1$). The corresponding vertical spectrum is

$$E_{\rm M}(k_z) \approx k_{\rm s}^2 \left(\frac{k_z}{k_{\rm s}}\right)^{-\beta_z}; \qquad \beta_z = (s-2)/H_z \quad (s > 2) \tag{20b}$$

(if $s<2$ then there is a high-wavenumber divergence; for finite high-wavenumber cut-off, $\beta_z=0$). Note that as required by the defining property of the spheroscale, the horizontal and vertical spectra are obviously equal when $k_z=K=k_{\rm s}$. We also note that here the elliptical dimension (eqs 12 and 17) is $d_{\rm el}=2+H_z$.

We can now calculate the spectrum of the surface magnetic field by substituting the above $P_{\rm M}$ into eq. (7); we obtain

$$\begin{aligned} E_{\rm B}(K) &= K^3 \int_{k_{\rm c}}^{k_i} \frac{dk_z}{|(\mathbf{K}, k_z)|^2 \|(\mathbf{K}, k_z)\|^s} \\ &= K^3 \int_{k_{\rm c}}^{k_i} \frac{dk_z}{(K^2 + k_z^2)[(K/k_{\rm s})^2 + (k_z/k_{\rm s})^{2/H_z}]^{s/2}}\,, \end{aligned} \tag{21}$$

where the lower limit $k_{\rm c}$ corresponds to the outer scale of the scaling region (the Curie depth) and $k_{\rm i}$ is the corresponding large-wavenumber (small, inner scale) cut-off. We note that if we replace the magnetization by rock density, the K^3 term by K and the magnetic field by the vertical component of gravity, we obtain the corresponding expression for the surface gravity spectrum [see Lovejoy *et al*. (2000), which shows that the theory presented here is compatible with empirical observations of surface gravity]. The analogy is particularly close here since we have essentially reduced the magnetization variability to a scalar rather than a vector problem (eliminating, for example, the need for a reduction to the poles). A more realistic scaling vector **M** theory is possible but beyond our present scope.

6 ESTIMATING H_z, s

6.1 Spectral analysis of susceptibility

The scaling behaviour of the integral (eq. 21) is fairly complicated, with many qualitatively different parameter ranges to consider (a near-complete analysis is given in Appendix A). Rather than exhaustively investigate all the different possible ranges, we therefore first consider how the parameters may be constrained by other information we have about the system, in particular by the statistics of magnetization. The data most

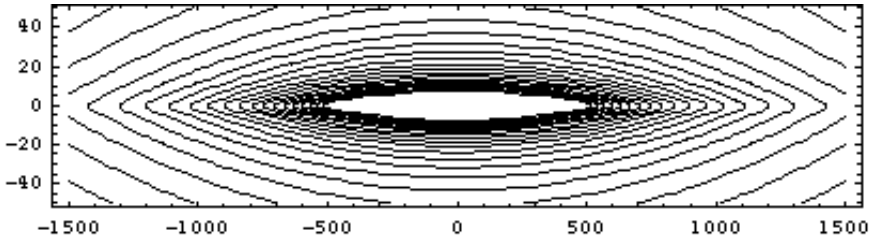

Figure 4. Vertical cross-section of isolines of the magnetization field structure function/variogramme in the crust (assuming the Curie depth $\approx$100 km); horizontal versus depth, $H_z=2$, spheroscale = 40 000 km. Scale in km, aspect ratio is 1/4. This is based on eq. (16b) and shows the typical magnetization structures that dominate the second-order statistics.

GJI 72960-8 10/1/01 13:13:08 Rev 6.05e/W (Mar 29 1999)
The Charlesworth Group, Huddersfield 01484 517077

15 readily available were not directly on the magnetization, but rather on the magnetic susceptibility (that is, we will ignore any remanent magnetization that may be present). If we assume isotropic magnetic *media*, then the magnetic susceptibilities are proportional to the induced magnetization and the latter are parallel to the inducing **B** field. Note that this is an assumption about the type of rock; the susceptibility tensor is assumed to be a scalar susceptibility multiplied by the identity/unit tensor. The field defined by the spatial distribution of scalar susceptibility is on the other hand assumed to be anisotropic and scaling. If we then ignore remanent magnetization (that is, assume that there is a low Königberger ratio, typical of continental crust), then the susceptibility can be used as a magnetization surrogate. The additional assumption adopted here is that over individual survey regions (which are all near the magnetic North Pole), the inducing **B** is roughly constant in direction (taken as the z-direction) so that the **M**, **B** relationship reduces to the scalar relation indicated by eq. (6).

With this in mind, we can therefore use the data for the magnetic susceptibility power spectra (both horizontal and borehole) from Pilkington & Todoeschuk (1993, 1995), kindly supplied by the authors to estimate magnetization statistics (Fig. 5). We see in the figure that for the two sets of horizontal susceptibility data there is reasonably good agreement with the 16 statistical fit to the high-wavenumber set, $B_x = 1.4$. Although the lower-wavenumber set is quite noisy, this value is roughly compatible with Pilkington & Todoeschuck's (1995) horizontal spectra. Note that although there is much variability in the borehole spectra depending on rock type, for igneous-type rock it is possible that the spheroscale is of the order of $10^4 - 10^5$ km (the location in Fig. 5 where the spectra would cross).

The susceptibility data are so noisy that it would be hazardous to guess the H_z that are obtained from the ratio of the (small) differences between the horizontal and vertical βs from the value $H_z = (\beta_x - 1)/(\beta_z - 1)$ (obtained by eliminating s from eqs 20a and b, although see the reference lines). In order to 17 obtain better estimates and more confidence that $H_z > 1$, we refer to Leary (1997), who has probably performed the most extensive analyses using both horizontal and vertical spectra from similar regions (he studied rock density, sound velocity and gamma emission). Due to strong (presumably multifractal) intermittency (see Marsan & Bean 1999), individual boreholes have a fair amount of spectral variability (recall that the spectrum is an ensemble-averaged quantity; the scaling is almost certainly violated on every individual realization).

The specific difficulty here in estimating H_z (and hence also the spheroscale) is that Leary's results were similar to those here, giving roughly $\beta_z \approx 1$, $\beta_x \approx 1$; his more precise analysis of 45 exponents (30 vertical, 15 horizontal) yields $\beta_z \approx 1.10 \pm 0.12$, $\beta_x \approx 1.34 \pm 0.12$, yielding $H_z \approx 3$ (to the nearest integer), a value that is roughly the same as the value for the magnetization (the two should be equal if Poisson's relation holds). Furthermore, elsewhere we analyse the susceptibility spectrum from the much longer KTB borehole finding, $\beta_z \approx 1.25$; similarly Shiomi *et al.* (1997) obtained $\beta_z \approx 1.1$–1.3 for susceptibilities of sedimentary rock and $\beta_z \approx 1.3$–1.6 for volcanic rock (see also Zhou & Thybo 1998). We also note that Leary gives nearly identical values for the exponents for rock density, gamma emission and sound velocity; this supports the idea that the value of H_z (and hence d_{el}) may be the same for different fields and hence supports the notion that it may be a fundamental characteristic of the geological stratification. Finally, by comparing rock densities

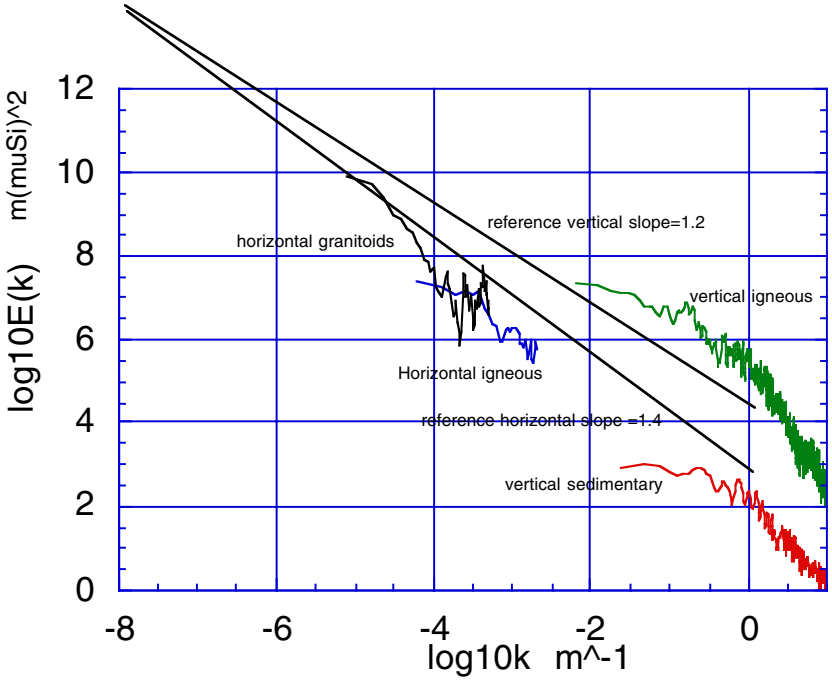

Figure 5. Power spectra of horizontal and vertical magnetic susceptibilities taken from Pilkington & Todoeschuk (1995) and Pilkington & Todoeschuk (1993), respectively [a typographic error in the measurement units in Pilkington & Todeschuck (1995) was corrected following a discussion with M. Pilkington]. The former have been multiplied by $2\pi k$ so as to yield angle-integrated rather than angle-averaged spectra. The straight lines show the reference slopes $\beta_x = 1.2$ (vertical), $\beta_x = 1.4$ (horizontal) with $H_z = (1.4\text{–}1)/(1.2\text{–}1) = 2$ and spheroscale at 10^5 km. Note that for the borehole data there is a large variation in spectral density depending on rock type, but that the vertical igneous and horizontal igneous do indeed show signs of intersecting at scales of 10^5 km or so, compatible with the indirect spheroscale estimates given by the model below. 37

GJI 72960-8 10/1/01 13:13:08 Rev 6.05e/W (Mar 29 1999)
The Charlesworth Group, Huddersfield 01484 517077

and surface gravity, Lovejoy *et al*. (2000) found that a similar value ($H_z \approx 3$) is compatible with gravity surveys, rock density statistics and theoretical analysis of density fluctuations in mantle convection. Although there is no compelling reason why H_z should be exactly the same for different rock properties, they are unlikely to be very different. This is because the various properties are correlated with each other, often assuming 'typical values' associated with different rock types. Since the classical picture of rock strata tends to identify different strata with different rock type, the degrees of stratification (H_z) cannot be too different (at least not for physically significant rock properties/parameters).

The small difference between the horizontal and vertical spectral exponents leads to poor estimates of H_z and also to great uncertainty in estimating the spheroscale. (Since the spheroscale is simply the scale where the horizontal variability equals the vertical variability, it is expected to vary greatly from place to place according to the local rock type; very large samples may be necessary for reasonable ensemble estimates.) Using Leary's spectra, we can attempt to estimate this scale by extrapolating to where the horizontal and vertical spectra would cross. Doing this using the above exponents, on Leary's graphs we find very rough estimates of ≈ 100 km, ≈ 1 m, ≈ 1 km, for rock density, gamma emission and velocity, but these are all quite inaccurate and presumably vary from place to place.

6.2 Spectral predictions of the model and comparison with magnetic field spectra

We have argued that the physically relevant case is that for which $h_z > 1$ and the Curie cut-off scale is much smaller than the spheroscale. Appendix A gives an estimate for the slopes of the two main spectral regions of $E_B(k)$ obtained from eq. (21),

$$\beta_h = s - 2, \qquad K > k_c,$$

$$\beta_i = s - 3, \qquad k_c > K > k_{ic}, \tag{22a}$$

where k_{ic} is the critical low-wavenumber cut-off for the intermediate scaling range,

$$k_{ic} = k_s (k_c / k_s)^{1/H_z}. \tag{22b}$$

A third very low-wavenumber regime also theoretically exists,

$$\beta_i = -3, K < k_{ic}, \tag{22c}$$

but is probably of sufficiently low wavenumber to be masked by the spectrum from the core (see below).

As we see, the slopes do not depend on H_z; the latter determines the width of the intermediate $\beta_i = s - 3$ regime (see Appendix A for details and see Fig. 6 for a schematic of the various ranges). From our earlier estimate of the slopes, $\beta_h \approx 2$ and $\beta_i \approx 1$ (see Fig. 1), we see that as predicted eq. (22) is respected (i.e. $\beta_h - \beta_h = 1$), with $s \approx 4$. Physically, the origin of the regimes is easy to understand; the following is justified in detail in Appendix A. At wavenumbers higher than the Curie wavenumber, we have the usual Spector–Grant type relation between the horizontal surface **B** spectrum and **M**; horizontal structures of wavenumber K are indeed dominated by vertical magnetization structures at wavenumber $k_z = K$. However, for $K < k_c$, this breaks down; Fig. 4 shows the geometrical reason. For this intermediate range, the horizontal surface **B** variability results from the contributions from thicker and thicker structures.

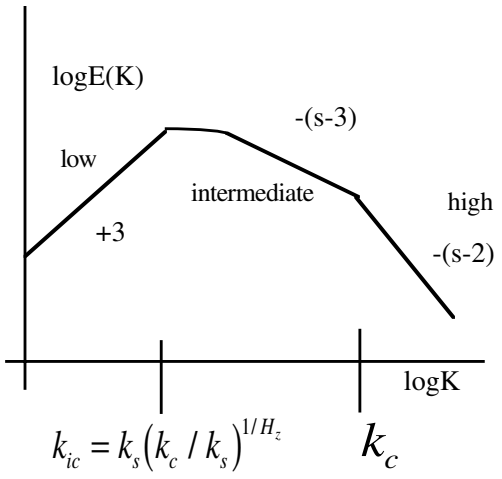

Figure 6. Schematic spectrum showing the scaling regimes in the case $H_z > 1$, $k_c > k_s$. As long as k_{ic} is less than about $(2000 \text{ km})^{-1}$, the low-wavenumber regime would be masked by the core contribution.

Finally, for horizontal structures corresponding to wavenumber $K = k_{ic}$, the thickest structures already span the entire magnetized region; the variability drops off very rapidly for lower wavenumbers ($\beta_l = -3$) since no new structures contribute.

We can now consider the (isotropic) limit $H_z \to 1$. We find that the intermediate (β_i) regime disappears and we obtain the Maus & Dimri (1995) result $\beta = \beta_h = s - 2$ for $K > k_c$, while for $K < k_c$, we obtain the $\beta_l = -3$ exponent. In other words, any isotropic scaling model will lead to a drastic low-wavenumber fall-off in the intermediate range spectrum, rather than the observed slow rise ($\beta_i \approx +1$). On the other hand, the existence of the intermediate spectral regime—which is so difficult to explain with classical models—is a generic feature of the anisotropic scaling models.

In order to obtain a value for H_z we now compare the horizontal and vertical susceptibility spectra in Fig. 5. Since the data are so sparse (the spectra are quite noisy), rather than using the best-fit regressions, we plot reference lines that are compatible with both Pilkington and Todeoschuck's data and with Leary's results, and (via eqs 20a and b) with the value of $s \approx 4$ found from the magnetic field data and eq. (21). For the vertical (borehole) data we have roughly slope $\beta_z \approx 1.2$ (particularly for the sedimentary rock) and $\beta_x \approx 1.4$ for the sedimentary rock with, therefore, $H_z \approx 2$, $s \approx 4.4$. However, the values $\beta_x \approx 1.3$, $\beta_z \approx 1.17$ (hence $H_z = 1.7$, $s = 4$) are just as good a compromise and were used for the simulations in Paper II (see Table 2 below).

Having an estimate of β_z and β_x, we may also make a rough estimate of the size of the spheroscale. At this scale, the horizontal and vertical spectra should intersect each other. Using the best spectra (from sedimentary vertical and horizontal boreholes), we estimate the intersection point at $k_s \approx 10^{-5}$ km^{-1}, or a spheroscale of approximately 100 000 km (this would imply, of course, that it is never attained). Using roughly these parameters, we can numerically integrate eq. (17) and compare the resulting theoretically predicted surface magnet field spectrum with the data. Figs 2 and 3 show that the result is in reasonable accord with values obtained from the anomaly spectra. Clearly, in order to make a better estimate of the spheroscale and s, H_z, susceptibility data from vertical and horizontal boreholes in the same region should be examined. Note that

18

GJI 72960-8 10/1/01 13:13:09 Rev 6.05e/W (Mar 29 1999)
The Charlesworth Group, Huddersfield 01484 517077

Table 2. A comparison of various theoretical and empirical constraints on the model parameters.

	H_z	s	β_x	β_z	$\beta_{\rm i}$	$\beta_{\rm h}$	$k_{\rm c}$	$k_{\rm s}$
Description	degree of stratification	exponent of spectral density of **M**	horizontal spectral exponent of **M**	vertical spectral exponent of **M**	low-wavenumber surface **B** spectral exponent	high-wavenumber surface **B** spectral exponent	Curie wavenumber (inverse Curie depth)	sphero-wavenumber (inverse spheroscale)
Theory	fundamental	fundamental	$s-H_z-1$	$(s-2)/H_z$	$s-3$ (1)	$s-2$	$k_{\rm s}<k_{\rm c}$	
Leary (1997) (2)	3	5.3	1.34 ± 0.12	1.10 ± 0.12				
Lovejoy *et al.* (2000) (3)	3	5.1						
data set # 1 (4)	2	3.6	0.6	0.8	0.6	1.6	$(30\ {\rm km})^{-1}$	$<(10^4\ {\rm km})^{-1}$ (5)
data set #2 (4)	2	4.4	1.4	1.2	1.4	2.4	$(100\ {\rm km})^{-1}$	$<(10^4\ {\rm km})^{-1}$ (5)
Other information	2 (6)	3.5–4. (7)					$(10\ {\rm km})^{-1}$–$(100\ {\rm km})^{-1}$ (8)	
Spectral model	1.7	4	1.30	1.17	1	2	$(10\ {\rm km})^{-1}$–$(100\ {\rm km})^{-1}$	$(10^{4.5}\ {\rm km})^{-1}$

(1) This intermediate-wavenumber regime extends down to $k_{\rm ic}=k_{\rm s}(k_{\rm c}/k_{\rm s})^{1/{\rm Hz}}$; there is then a very low-wavenumber regime with $\beta=-3$, which is probably swamped by the core contribution.
(2) These values for gamma emission, seismic velocity and rock density are given for comparison only. H_z is estimated from $H_z=(\beta_x-1)/(\beta_z-1)$.
(3) Exponents for rock density estimated from gravity surveys, rock density, theory of mantle convection; for comparison only.
(4) These were from roughly fitting numerical spectra; see Figs 2 and 3. The H_z dependence of the spectrum is only at all noticeable near the low-wavenumber end of the data; the fit is quite insensitive to this and to $k_{\rm s}$ as long as the critical wavenumber $k_{\rm ic}=k_{\rm s}(k_{\rm c}/k_{\rm s})^{1/{\rm Hz}}$ is $<(2000\ {\rm km})^{-1}$ (see Section 2).
(5) With $H_z=2$, the requirement that the low-wavenumber regime extends to $k_{\rm ic}=(2000\ {\rm km})^{-1}$ implies $k_{\rm s}<(10^5\ {\rm km})^{-1}$, $k_{\rm s}<(10^{4.5}\ {\rm km})^{-1}$ for $k_{\rm c}=(10^{1.5}\ {\rm km})^{-1}$, and $k_{\rm c}=(10^2\ {\rm km})^{-1}$, respectively.
(6) Numerical simulations in Paper II show that the ratio of the high- and low-wavenumber regime-**B** scaling exponents for low-order moments is H_z; the surface **B** data can then be used to estimate H_z, giving the value shown.
(7) Maus *et al.* (1997) obtained s in the range 3.5–4 for South African and Central Asian surface **B** spectra.
(8) Rough geothermal estimates assuming 20 K $\rm km^{-1}$ of vertical temperature gradient and a Curie temperature of 600 °C yields 30 km for the Curie depth. Due to local variations, the range indicated is more appropriate.

taking $k_s=(10^5\ \mathrm{km})^{-1}$, $k_c=(30\ \mathrm{km})^{-1}$, $H_z=2$, we estimate the low-wavenumber end of the $s-3$ (intermediate) range (k_{ic}; eq. 22b) to occur at $\approx(2000\ \mathrm{km})^{-1}$, which is roughly the high-wavenumber limit of the core contribution (see Figs 2 and 3). This would explain why the $\beta_l=-3$ crust regime is never observed; it would be negligible with respect to the core contribution.

6.3 Discussion of parameters and model/data comparison

At various points in this paper, we have appealed to theoretical considerations, and where possible, to empirical evidence to support our admittedly simple spectral model of crust magnetization, the key parameters being H_z, which controls the degree of stratification, and s, the exponent of spectral density P. In addition, there are two auxiliary model parameters (the size of the spheroscale, k_s^{-1} and the Curie depth, k_c^{-1}) but these are not very demanding on the model; the former need only be sufficiently large (see footnotes 4 and 5 to Table 2 below), while the latter need only be compatible with the geothermal profiles in the regions considered. The most stringent test of the model, therefore, derives from the fact that starting with the (H_z, s) pair, four other spectral exponents are derived: the horizontal and vertical magnetization exponents along with the high- and low-wavenumber surface **B** exponents. Since the best-quality data is that of the surface **B** field, probably the most convincing support for the model therefore comes from the fact that the theoretically predicted difference $\beta_h-\beta_i=1$ is reasonably well respected in Fig. 1 for both data sets #1, #2; this permits reasonable estimates of s, although even here the regional variations in s led to $s=4\pm0.4$ (that is, there is still substantial uncertainty, although the value $s=4$, hence $\beta_i=1$, $\beta_h=2$ is quite reasonable for both; see Fig. 1). The main difficulty is in obtaining a reasonable estimate of H_z, so the value 2 (used for example in Figs 2 and 3) is fairly *ad hoc*. In addition, the susceptibility data (used as a proxy for **M**) are extremely sparse, yielding exponents with large uncertainties. They are also uncomfortably close to the critical value 1 so that the estimate $H_z=(\beta_x-1)/(\beta_z-1)$ is particularly uncertain. Indeed, purely from the information discussed so far, perhaps the most convincing argument for an H_z in the vicinity of the value cited ($H_z\approx1.7$) is the fact that other related fields (including rock density) appear to have similar values of H_z. In the end, the most persuasive argument comes from the numerical multifractal simulations in Paper II, which enable us to compare all the statistical moments of the surface **B** field with the predictions of the model.

It is for these reasons that we have not attempted rigorous statistical parameter estimates, but rather tested for the compatibility of model parameters with the data. In order to help summarize the various empirical and theoretical constraints, we have constructed Table 2. The final line 'overall' is an admittedly somewhat subjective selection of most plausible all-round values.

7 CONCLUSIONS

The existence of fractal structures and scaling statistics can be understood as a natural consequence of scale-invariant geodynamical processes; their ubiquity has inspired numerous investigations into the scaling properties of the corresponding geophysical fields. This includes surface magnetism (**B**) and rock susceptibility (a surrogate for crustal magnetization, which is the source field for **B** at scales less than several thousand kilometres). However, still by far the most widespread framework for such scaling models and analyses is that of self-similar (isotropic) fields with unique fractal dimensions. These restrictions are serious obstacles to realistic theories and models of geofields. Self-similarity is unrealistic most notably because it ignores the fundamental role of stratification, while monofractality is simplistic because it ignores the role of intermittency (strong variability, the presence of anomalies). In this paper, we argue that the failure to account for stratification leads directly to a paradox for the surface **B** field: the inability to account simply and convincingly for the strong intermediate- range (≈2000 km to ≈100 km) 'red noise' variability in the surface **B** field. In comparison, a necessary consequence of the thinness of the magnetized crustal layer and of the large distance to the core is that self-similar models have a rapid ($\beta=-3$) low-wavenumber fall-off below the Curie wavenumber.

Classical potential theory shows that the surface **B** field is linearly determined by the volume **M** field, hence the latter is the physically more fundamental starting point for models; it also has the mathematical advantage of allowing for a unique determination of the surface **B** given the volume **M**. In addition, the second-order statistics (e.g. spectra) are particularly simply (linearly) related; we therefore restrict ourselves in Paper I to second-order statistical modelling. The basic assumption of the model is that the spectral density of the magnetization is scaling but anisotropic in the vertical plane, that is, the dynamical mechanism generating the magnetization distribution is scale-invariant but stratified. Additional (but secondary) assumptions are (a) that there exists a reference isoline of energy density whose shape is roughly spherical (at a Fourier space radius k_s, the spheroscale), and (b) that the (ensemble) spectral statistics are translationally invariant throughout the magnetized region (this is still compatible with enormous statistical variation from place to place on a single realization of the process). These assumptions determine the shape of the spectrum. Two additional simplifying assumptions were also made: (a) that the direction of the magnetization was constant over the region of interest, and (b) that the finite thickness of the magnetized layer (due to the Curie depth) can be approximated by a sharp Fourier space cut-off at the corresponding wavenumber k_c. These last two assumptions could be made more realistic, but would make only minor changes to the results.

The fundamental—and at first sight surprising—generic feature of the model is that the sharp Curie depth cut-off in the vertical **M** field does not lead to a cut-off in the horizontal spectrum of **B** spectra until (possibly) much, much lower wavenumbers. Instead, it produces a new intermediate scaling range 'red noise' spectrum whose exponent is one less than that of the high-wavenumber range. Although we exert a certain effort to obtain quantitative empirical estimates of the relevant parameters (notably the basic stratification parameter H_z and spectral scaling exponent s), because of the poverty of the magnetization surrogate (susceptibility) data, the most convincing vindication of the model is the excellent fit of the surface **B** spectra to the form predicted by the model (especially the change in slope of 1).

Systematic studies of magnetization statistics (in both horizontal and vertical directions) will clearly be needed to test the model further and provide more reliable parameter estimates (although see Table 2). However, even without waiting for this,

GJI 72960-8 10/1/01 13:13:11 Rev 6.05e/W (Mar 29 1999)
The Charlesworth Group, Huddersfield 01484 517077

two further tests of the anisotropic scaling are possible using the more abundant surface **B** data. The first is to go beyond second-order statistics and investigate the scaling of the statistics of all orders using multifractal analysis. The second is to make a multifractal model of **M** and to compare the surface **B** statistics with data. This is the subject of Paper II.

ACKNOWLEDGMENTS

We thank F. Francis, T. Falco and C. Hooge for help with some of the data analysis. M. Pilkington is especially thanked for supplying the magnetic survey data as well as the spectra from several of his publications. He also participated in many helpful discussions about the interpretation of aeromagnetic surveys and suggested many highly relevant references. We thank J. Todoeschuk for long discussions, and for critically commenting on an earlier draught. We also thank a referee (Prof. A. De Santis) for valuable suggestions for improving the manuscript. The Canadian Geological Commission is thanked for partial financial support.

REFERENCES

Bell, T.H., 1975. Statistical features of sea floor topography, *Deep Sea Res.,* **22,** 883–891.

Bills, B.G. & Kobrick, M., 1985. Venus topography: a harmonic analysis, *J. geophys. Res.,* **90,** 827–836.

Blakely, R.J., 1995. *Potential Theory in Gavity and Magnetic Applications,* Cambridge University Press, Cambridge.

Counil, J.L., Achache, J. & Galdeano, A., 1989. Long-wavelength magnetic anomalies in the Caribbean, plate boundaries and allochthonous continental blocks, *J. geophys. Res.,* **94,** 7419–7431.

Fedi, M., Quarta, T. & De Santis, A., 1997. Inherent power-law behaviour of magnetic field power spectra from a Spector and Grant ensemble, *Geophysics,* **62,** 1143–1150.

Fox, C.G. & Hayes, D., 1985. Quantitative methods for analyzing the roughness of the seafloor, *Rev. Geophys.,* **23,** 1–48.

Gregotski, M.E., Jensen, O. & Arkani-Hamed, J., 1991. Fractal stochastic models of aeromagnetic data, *Geophysics,* **56,** 1706–1715.

Harrison, C.G. & Carle, H.M., 1981. Intermediate wavelength magnetic anomalies over ocean basins, *J. geophys. Res.,* **86,** 11 585–11 599.

Harrison, C.G.A., Carle, H.M. & Hayling, K.L., 1986. Interpretation of satellite elevation magnetic anomalies, *J. geophys. Res.,* **91,** 3633–3650.

Klinkenberg, B. & Clarke, K.C., 1992. Exploring Fractal Mountains, in *Automated Pattern Analysis in Petroleum Exploration,* pp. 201–212, eds Palaz, I. & Sengupta, S.K., Springer-Verlag, Berlin.

Langel, R.A. & Estes, R.H., 1982. A geomagnetic field spectrum, *J. geophys. Res.,* **9,** 250–253.

Lavallée, D., Lovejoy, S., Schertzer, D. & Ladoy, P., 1993. Nonlinear variability and landscape topography: analysis and simulation, in *Fractals in Geography,* pp. 171–205, eds De Cola, L. & Lam, N., Prentice Hall, Place?.

Lazarev, A., Schertzer, D., Lovejoy, S. & Chigirinskaya, Y., 1994. Unified multifractal atmospheric dynamics tested in the tropics: part II, vertical scaling and generalized scale invariance, *Nonlinear Proc. Geophys.,* **1,** 115–123.

Leary, P., 1997. Rock as a critical-point system and the inherent implausibility of realizable earthquake prediction, *Geophys. J. Int.,* **131,** 451–466.

Lovejoy, S. & Schertzer, D., 1985. Generalized scale invariance in the atmosphere and fractal models of rain, *Water Resources Res.,* **21,** 1233–1250.

Lovejoy, S. & Schertzer, D., 1990. Our multifractal atmosphere: a unique laboratory for non-linear dynamics, *Can. J. Phys.,* **46,** 62.

Lovejoy, S. & Schertzer, D., 1995. How bright is the coast of Brittany?, in *Fractals in Geoscience and Remote Sensing,* pp. 102–151, ed. Wilkinson, G., Office for Official Publications of the European Communities, Luxembourg.

Lovejoy, S. & Schertzer, D., 1998. Stochastic chaos and multifractal geophysics, in *Chaos, Fractals and Models 96,* pp. 38–52, eds Guindani, F.M. & Salvadori, G., Italian University Press, Place?.

Lovejoy, S. & Schertzer, D., 1999. Stochastic chaos, symmetry and scale invariance, in *ECO-TEC, Architecture of the In-between,* pp. 80–99, ed. Marras, A., Princeton Architectural Press, Princeton, NJ.

Lovejoy, S., Lavallée, D. & Schertzer, D., 1995. Multifractal topography and the $l^{1/2}$ law, *Nonlinear Proc. Geophys.,* **2,** 17–22.

Lovejoy, S., Gaonac'h, H., Mareschal, J.C., Bourlon, E. & Schertzer, D., 2000. Anisotropic multiscaling models of rock density and the earth's surface gravity field, *J. geophys. Res.,* in press.

Lowes, F.J., 1974. Spatial power spectrum of the main geomagnetic field and extrapolation to the core, *Geophys. J. R. astr. Soc.,* **36,** 717–730.

Marsan, D. & Bean, J.C., 1999. Multiscaling nature of sonic velocities and lithography in the upper crystalline crust: evidence from the KTB main borehole, *Geophys. Res. Lett.,* **26,** 275–278.

Marsan, D., Schertzer, D. & Lovejoy, S., 1996. Causal space-time multifractal processes: predictability and forecasting of rain fields, *J. geophys. Res.,* **101,** 26 333–26 346.

Maus, S., 1999. Variogram analysis of magnetic and gravity data, *Geophysics,* **64,** 776–784.

Maus, S. & Dimri, V., 1995. Potential field power spectrum inversion for scaling geology, *J. geophys. Res.,* **100,** 12 605–12 616.

Maus, S. & Dimri, V., 1996. Depth estimation from the scaling power spectrum of potential fields?, *Geophys. J. Int.,* **124,** 113–120.

Maus, S., Gordon, D. & Fairhead, D., 1997. Curie-temperature depth estimation using a self-similar magnetization model, *Geophys. J. Int.,* **129,** 163–168.

Naidu, P., 1968. Spectrum of the potential field due to randomly distributed sources, *Geophysics,* **33,** 337–345.

Pecknold, S., 2000. Modeling anisotropic geophysical fields using generalized scale invariance and universal multifractals, *PhD thesis,* McGill University, Montréal.

Pecknold, S., Lovejoy, S. & Schertzer, D., 1997a. The morphology and texture of anisotropic multifractals using generalized scale invariance, in *Stochastic Models in Geosystems,* pp. xx–xx, eds Molchanov, S. & Woyczynski, W., Springer-Verlag, New York.

Pecknold, S., Lovejoy, S., Schertzer, D. & Hooge, C., 1997b. Multifractals and the resolution dependence of remotely sensed data: generalized scale invariance and geographical information systems, in *Scaling in Remote Sensing and Geographical Information Systems,* pp. 361–394, eds Quattrochi, D. & Goodchild, M., Lewis, Boca Raton.

Pecknold, S., Lovejoy, S. & Schertzer, D., 2000. Empirical investigation of topographic multiscaling, *Geophys. Res. Lett.,* in press.

Pflug, K., Lovejoy, S. & Schertzer, D., 1991. Generalized scale invariance, differential rotation and cloud texture, in *Nonlinear Dynamics of Structures,* pp. 71–80, eds Sagdeev, RZ., Frisch, U., Hussain, F., Moiseev, S.S. & Erokhin, N.S., Publisher?, Place?

Pilkington, M. & Todoeschuk, J.P., 1993. Fractal magnetization of continental crust, *Geophys. Res. Lett.,* **20,** 627–630.

Pilkington, M. & Todoeschuk, J., 1995. Scaling nature of crustal susceptibilities, *Geophys. Res. Lett.,* **22,** 779–782.

Pilkington, M., Gregotski, M. & Todoeschuk, J., 1994. Using fractal crustal magnetization models in magnetic interpretation, *Geophys. Prospect.,* **42,** 677–692.

Quarta, T., Fedi, M. & De Santis, A., 2000. Source ambiguity from estimation of the scaling exponent of potential field power spectra, *Geophys. J. Int.,* **140,** 311–323.

Schertzer, D. & Lovejoy, S., 1985a. The dimension and intermittency of atmospheric dynamics, in *Turbulent Shear Flows,* Vol. 4, pp. 7–33, Launder, B., Springer, Berlin.

Schertzer, D. & Lovejoy, S., 1985b. Generalised scale invariance in turbulent phenomena, *Phys. Chem. Hydrodyn. J.,* **6,** 623–635.

Schertzer, D. & Lovejoy, S., 1991. Nonlinear geodynamical variability: multiple singularities, universality and observables, in *Scaling, Fractals and Non-linear Variability in Geophysics,* pp. 41–82, eds Schertzer, D. & Lovejoy, S., Kluwer, Dordrecht.

Shiomi, K., Sato, H. & Ohtake, M., 1997. Broad-band power-law spectra of well-log data in Japan, *Geophys. J. Int.,* **130,** 57–64.

Spector, A. & Grant, F.S., 1970. Statistical models for interpreting aeromagnetic data, *Geophysics,* **35,** 293–302.

Stacey, F., 1992. *Physics of the Earth,* Brookfield Press, Brisbane.

Turcotte, D.L., 1989. Fractals in geology and geophysics, *Pageoph,* **131,** 171–196.

Van Zandt, T.E., Smith, S.A., Tsuda, T., Fritts, D.C., Sato, T., Fukao, S. & Kato, S., 1990. Studies of velocity fluctuations in the lower atmosphere using the mu radar, Part I: azimuthal anisotropy, *J. Atmos. Sci.,* **47,** 39–50.

Venig-Meinesz, F.A., 1951. A remarkable feature of the Earth's topography, *Proc. K. Ned. Akad. Wet. Ser. B Phys. Sci.,* **54,** 212–228.

Wasilewski, P. & Mayhnew, M., 1992. The moho as a magnetic boundary revisited, *Geophys. Res. Lett.,* **19,** 2259–2262.

Weissel, J.K. & Pratson, L.F., 1994. The length scaling properties of topography, *J. geophys. Res.,* **99,** 13 997–14 012.

Zhou, S. & Thybo, H., 1998. Power spectra analysis of aeromagnetic data and KTB susceptibility logs, and their implications for fractal behaviour of crustal magnetization, *Pageoph,* **151,** 147–159.

APPENDIX A: SCALING REGIMES FOR THE SURFACE B FIELD

In Section 5 (eq. 21), the energy spectrum of the z-component of the surface **B** field ($E_B(K)$) was given under the assumption that the magnetization has only a z-component and has scaling stratification,

$$E_B(K) = K^3 \int_{k_c}^{k_i} \frac{dk_z}{(K^2+k_z^2)[(K/k_s)^2+(k_z/k_s)^{2/H_z}]^{s/2}}, \qquad \text{(A1)}$$

where K is the modulus of the horizontal wavenumber, H_z characterizes the degree of stratification and k_s is the scale where the magnetization has the same variance in both the horizontal and the vertical directions (the 'spheroscale'). The upper limit of integration k_i (corresponding in physical space to the inner scale of the vertical scaling of the magnetization) turns out not to be important for the parameters of interest here. However, we will see that the lower limit (k_c, corresponding to the outer limit of vertical scaling in physical space, the Curie wavenumber) is very important. This abrupt Fourier space cut-off (corresponding to a 'sinc' function real-space cut-off) is an admittedly crude approximation to what is presumably a fractal bottom cut-off of the magnetized region associated with the Curie temperature/depth.

Although Table A1 covers the complete parameter range, the detailed derivations in the following are for the physically relevant case $H_z>1$ (corresponding to horizontal stratification increasing towards smaller scales). The evidence for $H_z>1$ comes from various horizontal and vertical data sets (see the discussion in Section 6, including the susceptibility spectra shown in Fig. 5, especially Table 2). An additional fairly general argument can be made simply from the observation that the spectral energy at scales of kilometres is apparently larger in the vertical direction than in the horizontal at the same scales. This means that the smaller and smaller scales will be increasingly stratified only if $H_z>1$. Less directly, Lovejoy *et al.* (1999) showed that a rock density field (presumably related to the magnetization, e.g. by Poisson's relation) with $H_z>1$ can explain the surface gravity spectrum. In addition, the success of spectral modelling the surface **B** field with this assumption (Figs 2 and 3) or multifractal simulations (Section 6) gives this assumption *a posteriori* justification.

Table A1. The various high- and low-wavenumber exponents for $s>-H_z$, $H_z>0$. The case of interest here is the first column.

β_i	$s-1-H_z$	$\left(\frac{s}{H_z}-2\right)$	$(s-2)$
	$s>H_z>1$	$H_z>s>1$	$H_z<1$
β_h	$(s-2)$	$s-3+H_z$	$\left(\frac{s}{H_z}-2\right)$
	$H_z>1$	$s>H_z$; $H_z<1$	$s<H_z<1$

Given $H_z>1$, the two main cases to consider depend on whether or not the Curie depth is relevant.

(1) The Curie depth is unimportant: $k_c \ll k_s$

This is the simplest case where the Curie depth is effectively infinite and allows us to understand more easily the case where the finite Curie depth is taken into account.

(i) High-wavenumber end: $K>k_s$

In this spectral domain, since $H_z>1$, we have $K<k_s(K/k_s)^{H_z}$ so that we obtain from eq. (A1)

$$E_B(K) \approx \int_{k_c}^{K} K^{-s+1}k_s^s dk_z + \int_{K}^{k_s(K/k_s)^{H_z}} K^{3-s}k_s^s k_z^{-2} dk_z + \int_{k_s(K/k_s)^{H_z}}^{\infty} K^3 k_s^{s/H_z} k_z^{-2-s/H_z} dk_z \qquad \text{(A2a)}$$

with the restriction $s>-H_z$ (otherwise there is a high-wavenumber divergence). This yields two dominant terms of the form

$$k_s^2\left(\frac{K}{k_s}\right)^{2-s}, \qquad k_s^2\left(\frac{K}{k_s}\right)^{3-s-H_z} \qquad \text{(A2b)}$$

for the low-k_z and high-k_z regions, respectively. Recalling that in this regime $K>k_s$, the term with the largest exponent will dominate; since we have also assumed $H_z>1$, the first term dominates. This implies that $\beta_h=s-2$ and most of the dominant contribution to the high-wavenumber $E_B(K)$ comes from $k_z \approx K$.

(ii) Low-wavenumber end: $K<k_s$

Here we have $K>k_s(K/k_s)^{H_z}$ so that we obtain

$$E_B(K) \approx \int_{k_c}^{k_s(K/k_s)^{H_z}} K^{-s+1}k_s^s dk_z + \int_{k_s(K/k_s)^{H_z}}^{K} K^1 k_s^{s/H_z} k_z^{-s/H_z} dk_z + \int_{K}^{\infty} K^3 k_s^{s/H_z} k_z^{-2-s/H_z} dk_z \qquad \text{(A3)}$$

GJI 72960-8 10/1/01 13:13:11 Rev 6.05e/W (Mar 29 1999)
The Charlesworth Group, Huddersfield 01484 517077

with the same restriction $s > -H_z$. We obtain terms with the following scaling:

$$k_s^2\left(\frac{K}{k_s}\right)^{2-s/H_z}, \qquad k_s^2\left(\frac{K}{k_s}\right)^{1+H_z-s}. \tag{A4}$$

Recalling that $K<k_s$, the dominant term now has the smallest exponent and we find that the first term dominates for $s<H_z$, whereas the second term dominates for $s>H_z$; the latter is the relevant case here. Note that in the case $s>H_z$, this implies that the dominant contribution to the low-wavenumber horizontal spectrum comes from $k_z \approx k_s(K/k_s)^{H_z}$.

In summary, if k_c is small enough, since we will see that typical values of empirical βs easily satisfy $s>H_z-1$, we are interested in the formulae

$$\beta_i = s - H_z - 1, \qquad \beta_h = s - 2.$$

We see that both the high- and low-k_z cut-offs are unimportant. Convenient formulae for H_z, s are therefore

$$H_z = \beta_h - \beta_i + 1,$$

$$s = \beta_h + 2.$$

Taking the (isotropic) limit $H_z \to 1$, we obtain $\beta_i = \beta_h = s-2$, which is a result derived in Maus & Dimri (1995).

Finally, we found that the integrals are dominated by the contribution at $k_z = K$ for $K>k_s$, but for $K<k_s$ they are dominated by $K = k_s(K/k_s)^{H_z}$. This is a statistical one–one relation between horizontal statistics and vertical statistics, a generalization of the deterministic-type relations sought by Spector & Grant (1970) (and used for determining depths of sources in prospecting). Translated into real space terms, it means that

$$\Delta z \approx l_s\left(\frac{\Delta x}{l_s}\right)^{H_z} \qquad \Delta x < l_s,$$

$$\Delta z \approx \Delta x \qquad \Delta x > l_s, \tag{A5}$$

where $l_s = 1/k_s$ is the spheroscale and Δz is the thickness of the layer in the vertical contributing to the horizontal structures in the magnetic map of scale Δx. Note that since the contribution from a layer depth z decreases exponentially (as $e^{-K|z|}$; see eq. 4b), it would appear to be legitimate to consider that the dominant structure of vertical extent Δz is in fact roughly situated between the surface and depth z. Hence, this analysis gives support to the existence of relations between horizontal extent and depth, except that (a) the relationship is only statistical and (b) it is the non-standard two scaling regime formula above. In fact, we find that for the low-wavenumber regime, the Curie depth is dominant (the low-wavenumber regime is apparently not physically relevant), so that these conclusions only hold for the high-wavenumber regime.

(2) Curie depth is important, $k_c > k_s$

In this (physically relevant) case, we can use the same approximations as before (breaking the integral into three zones depending on k_z as before). The interesting case is $K>k_s$ and we obtain three zones,

$$E_B(K) \approx \int_{k_c}^{K} K^{-s+1} k_s^s dk_z \approx K^{2-s} k_s^s, \qquad K > k_c,$$

$$E_B(K) \approx \int_{k_c}^{k_s(K/k_s)^{H_z}} K^{3-s} k_s^s k_z^{-2} dk_z$$

$$\approx K^{3-s} k_s^s k_c^{-1}, \qquad k_c > K > k_s(k_c/k_s)^{1/H_z}, \tag{A6}$$

$$E_B(K) \approx \int_{k_c}^{\infty} K^3 k_s^{s/H_z} k_z^{-2-s/H_z} dk_z$$

$$\approx K^3 k_s^{s/H_z} k_c^{-1-s/H_z}, \qquad K < k_s(k_c/k_s)^{1/H_z}.$$

These are the very low-, low- and high-wavenumber regimes,

$$\beta_i = -3, \beta_i = s-3, \qquad \beta_h = s-2. \tag{A7}$$

It is only the last two that are physically significant. A numerical example is shown in Fig. A1.

The important point to note is that the existence of anisotropic scaling manifests itself as a change in slope of 1 between the high and intermediate regions. Only the length of the region depends on the value of H_z, not the slopes. The maximum occurs at roughly $k_s(k_c/k_s)^{1/H_z}$.

We now examine the relation between the high- and low-wavenumber magnetization and magnetic field statistics. We note that in eq. (A6) for $K>k_c$, the dominant contribution to $E_B(K)$ comes from $k_z \approx K$, whereas for $K<k_c$ it comes from $k_z \approx k_c$, implying that all vertical scales are important and a Spector–Grant type identification of horizontal **B** anomalies with sources at specific depths is no longer possible. To better understand the statistical relations between **B** and **M**, we may use these approximations to rewrite eq. (A6) as follows:

$$P_B(K) \approx K^2 P_M(K, 0), \qquad K > k_c,$$

$$P_B(K) \approx K P_M(K, 0), \; K < k_c. \tag{A8}$$

Since P is quadratic in Fourier transforms, this implies—at least as far as the spectra are concerned—that the surface **B** field has the same statistical properties as the vertically integrated magnetization ($\mathbf{M}(K, 0)$) filtered by K and $K^{1/2}$ for

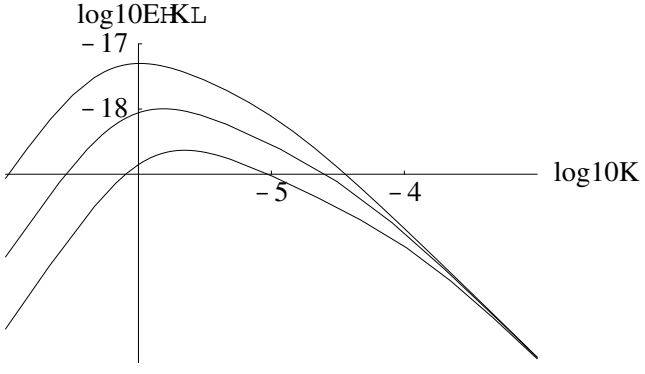

Figure A1. Numerical integration of eq. (A1) with parameters $k_s = 10^{-7}$, $s=4$, $H_z=3$ showing the effect of varying the Curie depth $k_c = 10^{-4}$, $10^{-4.5}$, 10^{-5} (bottom to top). The three regimes are clearly shown with $\beta_l = -3$, $\beta_i = 1$, $\beta_h = 2$.

GJI 72960-8 10/1/01 13:13:12 Rev 6.05e/W (Mar 29 1999)
The Charlesworth Group, Huddersfield 01484 517077

the high- and low-wavenumber regimes, respectively. This corresponds to fractional differentiation of order 1 and 1/2, respectively.

Since $\beta_h = s-2$, $\beta_i = s-3$, a change in slope of 1 at the Curie/ 41
cut-off depth is thus a fundamental prediction of the model and the reasonable agreement between this prediction and the surface **B** field is in itself strong support for the model. This special low-wavenumber scaling regime—which is a unique prediction of the anisotropic scaling model—explains in a simple way the 'intermediate range' of magnetic anomalies (those shorter than the core contribution (approximately 2000 km) but longer than the Curie depth (approximately 10–100 km).

APPENDIX B: HORIZONTAL ANISOTROPY AND SPURIOUS SCALING BREAKS

If the magnetic anomaly field is scaling but non-self-similar then the use of isotropic analysis techniques (such as isotropic energy spectra or isotropic trace moments; see Paper II) will generally lead to spurious breaks in the scaling. We examine here the magnitude of such effects and demonstrate that they are not responsible for the break in Fig. 1.

First consider the general form of a scaling spectral density $P(\mathbf{k})$ given by eq. (14). To quantify the effect of overall stratification on the isotropic spectrum, consider the simple self-affine case where the stratification occurs in orthogonal directions; take **G** as a diagonal matrix with $d=1$ and $e=f=0$. (The rotation dominance case involves sinusoidal modulations of the spectrum with a constant logarithmic period equal to $2\pi/|a|$ so that there is no overall break of the sort observed in Fig. 1.) A spectral density respecting this anisotropic scaling (eq. 14) is

$$P(k_x, k_y) = \left(\left(\frac{k_x}{k_s}\right)^{2/(1+c)} + \left(\frac{k_y}{k_s}\right)^{2/(1-c)} \right)^{-s/2}, \qquad \text{(B1)}$$

where k_s is the wavenumber of the 'spheroscale'. In two dimensions, the usual (isotropic) energy spectrum $E(k)$ (where $k^2 = k_x^2 + k_y^2$) is obtained by integrating P over circles,

$$E(K) = K \int_0^{2\pi} \frac{d\theta}{[(K\cos\theta/k_s)^{2/(1+c)} + (K\sin\theta/k_s)^{2/(1-c)}]^{s/2}} \qquad \text{(B2)}$$

(since $k_x = K\cos\theta$, $k_y = K\sin\theta$). In self-similar systems (eq. B2 with $c=0$), we recover the usual result: the spectral exponent $\beta = s-1$. In D dimensions, the relation is $\beta = s-D+1$.

We may now consider $E(k)$ for $c \neq 0$; in this case, it is not hard to show that we obtain two different asymptotic scaling regimes (for $k \ll k_s$, $k \gg k_s$). Denoting the corresponding spectral exponents by β_l, β_h, we obtain the cases listed in Table B1.

Table B1. The various high- and low-wavenumber scaling isotropic spectral exponents for the spectral density eq. (B2). For more general linear GSI it suffices to replace c by a.

	$s<1-\lvert c\rvert$	$1-\lvert c\rvert<s<1+\lvert c\rvert$	$s>1+\lvert c\rvert$
β_h ($k \gg k_s$)	$-1+\frac{s}{1-\lvert c\rvert}$	$1+\frac{s-2}{1+\lvert c\rvert}$	$1+\frac{s-2}{1+\lvert c\rvert}$
β_l ($k \ll k_s$)	$-1+\frac{s}{1+\lvert c\rvert}$	$-1+\frac{s}{1+\lvert c\rvert}$	$1+\frac{s-2}{1-\lvert c\rvert}$

The extension of this result to the general stratification dominance case (i.e. $a^2>0$ but $f\neq 0$, $e\neq 0$) is straightforward 42
since the stratification is now along (non-orthogonal) directions (the eigenvectors of **G**). We can therefore choose the same form for P except that k_x, k_y refer to non-orthogonal coordinates and we simply replace c by a (since $\pm a$ are the eigenvalues of the traceless part of **G**). With these changes, we recover the same asymptotic scaling regimes as those shown in Table 3. 43

In order to explain the break in Fig. 1 by invoking scaling anisotropy in the horizontal magnetic anomaly field, we could use estimates of β_l and β_h to invert the two above equations to determine s and a. Direct estimates of a, given in Paper II, indicates fairly small values of a, at most 0.24. This would yield a break of at most about $\Delta\beta \approx 0.5$, smaller than observed by a factor of 2. Additionally, in most cases the (horizontal) spheroscale is quite small; thus, this effect would not be observed at all in the data sets used for Fig. 1.

GJI 72960-8 10/1/01 13:13:13 Rev 6.05e/W (Mar 29 1999)
The Charlesworth Group, Huddersfield 01484 517077

AUTHORS QUERIES

Journal: GJI
Paper: 1344

Dear Author
During the preparation of your manuscript for publication, the questions listed below have arisen. Please attend to these matters and return this form with your proof. Many thanks for your assistance

Query Reference	Query	Remarks
1	**Au: wide ranging**	
2	**Au: a or b?**	
3	**Au: a or b?**	
4	**Lavallee et al. 1993** has been changed to **Lavallée et al. 1993** so that this citation matches the list	
5	Au: Is the text OK: **we conclude**	
6	**Au: please check carefully that ALL maths has been set correctly**	
7	**Au: show?**	
8	**Au: bold OK?**	
9	**Au: OK?**	
10	Au: Is the text OK: **is done so by**	
11	**Au: This is not a complete sentence**	
12	**Schertzer & Lovejoy 1985b** has been changed to **Schertzer 1985b** so that this citation matches the list	

13	**Lovejoy et al. 1999** has been changed to **Lovejoy & Schertzer 1999** so that this citation matches the list	
14	**Pecknold et al. 1996** has been changed to **Pecknold et al. 1997** so that this citation matches the list **a or b?**	
15	Au: What do you mean by the following text: **directly on**?	
16	Au: Is the text OK: **Bx = 1.4**	
17	Au: What do you mean by the following text: **see the reference lines**?	
18	**Au: magnetic?**	
19	Au: Is the text OK: **summarize the**	
20	Au: What do you mean by the following text: **final line 'overall'**?	
21	Au: Is the text OK: **Cambridge**	
22	Au: Is the text OK: **Berlin**	
23	**Au: Place?**	
24	**Au: Place?**	
25	**Au: Any update?**	
26	Au: Is the text OK: **1997a**	
27	**Au: page range?**	
28	Au: Is the text OK: **1997b**	
29	**Au: Any update?**	
30	**Au: Publisher?, Place?**	

31	**Quarta et al. 2000** has not been found in the text	
32	Au: Is the text OK: **Berlin**	
33	**Au: #2**	
34	**Au: please check punctuation within bracket: the original was a bit confusing**	
35	**Au: please check punctuation within bracket: the original was a bit confusing**	
36	Au: What do you mean by the following text: **horizontal versus depth**?	
37	Au: What do you mean by the following text: **model below**?	
38	**Au: at depth?**	
39	Au: Is the text OK: **two scaling regime**	
40	Au: Is the text OK: **very low-, low- and high-wavenumber**	
41	Au: Is the text OK: **between**	
42	Au: What do you mean by the following text: **now along (non-orthogonal) directions**?	
43	**Au: There is no Table 3**	

Offprints – Order Form 2001

A PDF file will be supplied to authors upon publication of their article. There are no free offprints and copies are only available if this order form is returned within seven days of receipt.

Purchasing Copies
You may order additional offprint copies. Prices are listed below, and include postage & packing. Payment is required by a cheque (drawn on a UK clearing bank) sent with order, credit card, or an official purchase order. A purchase order will only be accepted if it is issued by your employer, organisation or funding institution. Offprints purchased by this method are payable 30 days from the date of invoice.

Delivery
Offprints are despatched by Surface Mail about three weeks after publication. Overseas orders can take up to six weeks before you receive the copies.

Scale of prices for Offprints
These prices are valid for up to 500 copies for author use only and must not be used for commercial sales. Please obtain a quotation for more than 500 copies. In addition, these prices are only valid for orders received before the publication is in press. Orders received thereafter will have to be reprinted specially, and will therefore be more expensive.

Local tax rates are: Belgium 6%; France 2.1%; Germany 7%; The Netherlands 6%, Spain 4% and should be added to each order unless a local tax registration number is provided.

Journal GJI ..... First Author S. Lovejoy .....

Paper no 1344 ..... pp .....

Short title Stratified multifractal magnetization—I .....

Please complete in block capitals
Name and Address (for delivery of Offprints; no PO Box numbers if possible)

.....

.....

.....

.....

..... City ..... Country .....

Address for invoicing (if appropriate)

.....

.....

.....

Telephone No..... Fax No..... email address..... .....

I wish to order ..... (minimum 50) additional Offprints Value ..... + local EC VAT (if applicable)

Please send my copies by air mail (add 15% to cost)

I wish to order ..... (minimum 50) Coloured Card Covers, colour (please state) .....

Value .....

I enclose payment by cheque for .....

Payment by Credit Card (Mastercard/VISA/American Express/Diners Club)

Please debit my card number .....

Expiry Date ..... / ..... with the sum of .....

Signature ..... Date .....

Card address, if different from delivery address above:

.....

.....

.....

Purchase order details .....

I attach order number ..... dated .....

EC VAT number (if applicable)
Please note failure to include your EC VAT registration number at the time of order will result in an administration fee of £35 to amend invoices.

This order covers all requirements for Offprints of my paper, and I agree that all original material submitted to the journal for this paper can be destroyed after six months unless I request its return within that period.

Signed ..... Date .....

Please tick 4 if this is a confirmation of faxed order o

All orders/queries regarding this order should be addressed (within seven days) to:
Offprints Dept, Blackwell Science Ltd, Osney Mead, Oxford OX2 0EL, United Kingdom
Telephone: +44 (0)1865 206206
Fax: +44 (0)1865 206189
email: offprints@blacksci.co.uk

Blackwell Science Journals

Offprints

2001 PRICES

(The following EC countries must add local tax unless a registration number is provided – Belgium, France, Germany, The Netherlands and Spain)

Sterling Prices

COPIES	1–4pp	5–8pp	9–12pp	13–16pp	17–20pp	21–24pp	25–28pp	29–32pp
50	86.00	113.00	139.00	235.00	315.00	374.00	432.00	490.00
100	143.00	184.00	238.00	238.00	386.00	460.00	533.00	607.00
150	208.00	250.00	291.00	371.00	478.00	568.00	659.00	748.00
200	261.00	309.00	357.00	434.00	561.00	666.00	773.00	878.00
250	298.00	351.00	402.00	501.00	641.00	763.00	886.00	1007.00
300	339.00	393.00	457.00	570.00	723.00	861.00	998.00	1137.00
400	417.00	475.00	565.00	704.00	886.00	1057.00	1226.00	1395.00
500	470.00	547.00	675.00	838.00	1040.00	1238.00	1439.00	1640.00

A choice of coloured card covers are also available. Colours: cream, red, green, blue, white.
Prices: 50 – £224.00; 100 – £256.00; 50 run on – £32.00; 100 run on – £55.00

US Dollar Prices

COPIES	1–4pp	5–8pp	9–12pp	13–16pp	17–20pp	21–24pp	25–28pp	29–32pp
50	132.44	174.02	214.06	361.90	485.10	575.96	665.28	754.60
100	220.22	283.36	366.52	466.62	594.44	708.40	820.82	934.78
150	320.32	385.00	448.14	571.34	736.12	874.72	1014.86	1151.92
200	401.94	475.86	549.78	668.36	863.94	1025.64	1190.42	1352.12
250	458.92	540.54	619.08	771.54	987.14	1175.02	1364.44	1550.78
300	522.06	605.22	703.78	877.80	1113.42	1325.94	1536.92	1750.98
400	642.18	731.50	870.10	1084.16	1364.44	1627.78	1888.04	2148.30
500	723.80	842.38	1039.50	1290.52	1601.60	1906.52	2216.06	2525.60

A choice of coloured card covers are also available. Colours: cream, red, green, blue, white.
Prices: 50 – $344.96; 100 – $394.24; 50 run on – $49.28; 100 run on – $84.70

MARKED PROOF

Please correct and return this set

Please use the proof correction marks shown below to indicate all alterations and corrections required in your proof.

Instruction to printer	*Textual mark*	*Marginal mark*
Leave unchanged	··· under matter to remain	Stet
Insert in text the matter indicated in the margin	⅄	New matter followed by ⅄
Delete	⊢ through matter to be deleted	⅁
Delete and close up	⊖ through matter to be deleted	⅁
Substitute character or substitute part of one or more word(s)	/ through letter or ⊢ through word	New letter or new word
Change to italics	— under matter to be changed	⌊⌊
Change to capitals	≡ under matter to be changed	≡
Change to small capitals	= under matter to be changed	=
Change to bold type	~ under matter to be changed	~
Change to bold italic	≈ under matter to be changed	⌊~
Change to lower case	Encircle matter to be changed	≠
Change italic to upright type	(As above)	⌐⌊
Insert 'superior' character	/ through character or ⅄ where required	Y under character e.g. Y
Insert 'inferior' character	(As above)	⅄ over character e.g. ⅄₂
Insert full stop	(As above)	⊙
Insert comma	(As above)	,
Insert single quotation marks	(As above)	⅋ and/or ⅋
Insert double quotation marks	(As above)	⅋⅋ and/or ⅋⅋
Insert hyphen	(As above)	(hy)
Start new paragraph	⌐	⌐
No new paragraph	⌒	⌒
Transpose	⌐⌐	⌐⌐
Close up	linking ⊂ letters	⊂
Insert space between letters	⅄ between letters affected	#
Insert space between words	⅄ between words affected	#
Reduce space between letters	⊤ between letters affected	⊤
Reduce space between words	⊤ between words affected	⊤